CHEMISTRY

Exploiting equilibrium-kinetic synergetic effect for separation of ethylene and ethane in a microporous metal-organic framework

Qi Ding[1,2], Zhaoqiang Zhang[1], Cong Yu[1], Peixin Zhang[3], Jun Wang[3], Xili Cui[1,2], Chao-Hong He[1,2], Shuguang Deng[4], Huabin Xing[1,2]*

Physisorption is a promising technology to cut cost for separating ethylene (C_2H_4) from ethane (C_2H_6), the most energy-intensive separation process in the petrochemical industry. However, traditional thermodynamically selective adsorbents exhibit limited C_2H_4/C_2H_6 selectivity due to their similar physiochemical properties, and the performance enhancement is typically at the expense of elevated adsorption heat. Here, we report highly-efficient C_2H_4/C_2H_6 adsorption separation in a phosphate-anion pillared metal-organic framework $ZnAtzPO_4$ exploiting the equilibrium-kinetic synergetic effect. The periodically expanded and contracted aperture decorated with electronegative groups within $ZnAtzPO_4$ enables effective trapping of C_2H_4 and impedes the diffusion of C_2H_6, offering an extraordinary equilibrium-kinetic combined selectivity of 32.4. The adsorption heat of C_2H_4 on $ZnAtzPO_4$ (17.3 to 30.0 kJ mol^{-1}) is substantially lower than many thermodynamically selective adsorbents because its separation capability only partially relies on thermodynamics. The separation mechanism was explored by computational simulations, and breakthrough experiments confirmed the excellent C_2H_4/C_2H_6 separation performance of $ZnAtzPO_4$.

INTRODUCTION

As an important feedstock in petrochemical industries, ethylene (C_2H_4) is one of the highest-yield chemicals in the world with a global production capacity of more than 170 million tons in 2016 (*1*). C_2H_4 is usually manufactured by steam cracking and thermal decomposition of naphtha or ethane (C_2H_6), and the product inevitably contains a certain amount of C_2H_6 impurity. To obtain polymer-grade C_2H_4 as the raw material for downstream high value-added products, it is necessary to remove the residual C_2H_6, which is a challenging task due to the very close molecular size of C_2H_6 (3.81 Å × 4.08 Å × 4.82 Å) and C_2H_4 (3.28 Å × 4.18 Å × 4.84 Å) and their similar physical properties (*2*, *3*). Industrial separation of C_2H_4 and C_2H_6 is generally realized by energy-intensive cryogenic distillation that requires very harsh operation conditions (*4*), typically at temperature as low as −90° to −15°C and pressure up to 23 bar under a high reflux ratio in distillation towers installed with more than 150 trays (*5*). The energy used for C_2H_4/C_2H_6 and C_3H_6/C_3H_8 separation accounts for more than 0.3% of the global energy consumption; therefore, developing energy-efficient methods for C_2H_4/C_2H_6 separation is highly demanded and is recognized as one of the most important industrial tasks to change the world's energy footprint (*6*).

Adsorption separation enabling efficient gas purification under mild conditions is an energy-saving alternative technology to cryogenic distillation (*7*–*13*), and the key lies in developing advanced porous materials (*14*–*16*). With regard to C_2H_4/C_2H_6 separation, introducing transition-metal ions and unsaturated metal sites into the adsorbents has been widely accepted as a feasible approach (*5*, *17*–*21*), because they can selectively interact with π-electrons of C_2H_4 molecules. However, the π-complexation–related materials generally present limited stability, especially in the presence of moisture and sulfides (*22*), and demand high energy cost for the adsorbents' regeneration because of their strong affinity to C_2H_4 (*23*). Porous materials that are amenable to achieve complete molecular sieving are ideal for C_2H_4/C_2H_6 separation (*24*). However, to precisely control aperture size to a critical range necessary to exclude C_2H_6 is very challenging, and pores with such limited size typically lead to low diffusion rate and gas uptake. Considering that a practical separation process is simultaneously controlled by effects that arise from thermodynamics and kinetics, adsorbents that can exploit both equilibrium and kinetic selectivity are appealing for gas capture and purification (*25*, *26*) but intractable to design and prepare. Previously, most porous materials reported for C_2H_4/C_2H_6 separation are principally based on their discrepant thermodynamic affinity for the guests (*27*–*30*). Only a few of zeolites and coordination polymer have been described as suitable substances for kinetic separation (*31*–*33*), largely because the analogous dimensions of C_2H_4 and C_2H_6 bring critical difficulty to fabricate pores with appropriate sizes that permit the passing of C_2H_4 while limiting the diffusion of slightly bulkier C_2H_6 molecules. Moreover, the ultimate efficiencies of reported kinetically selective adsorbents are basically confined by disadvantageous thermodynamic effects, in which case the capacity of C_2H_6 at the equilibrium state is quite close to or even exceeds that of C_2H_4 under a wide pressure range. These observations suggest that there is still a broad space to further enhance the separation of C_2H_4 and C_2H_6 by developing porous materials with optimal adsorption thermodynamics and kinetics.

Here, we reveal the high-efficient separation of C_2H_4 and C_2H_6 in a phosphate-anion (PO_4^{3-}) pillared metal-organic framework (MOF) $\{Zn_3(Atz)_3(PO_4)\}_\infty$ ($ZnAtzPO_4$; Atz = 3-amino-1,2,4-triazole) by exploiting synergetic effect of equilibrium and kinetics. The material features periodically expanded and contracted pore decorated by electronegative groups, which provides sufficient binding sites for

[1]Key Laboratory of Biomass Chemical Engineering of Ministry of Education, College of Chemical and Biological Engineering, Zhejiang University, Hangzhou 310027, China. [2]Institute of Zhejiang University—Quzhou, 78 Jiuhua Boulevard North, Quzhou 324000, China. [3]School of Resource, Environmental and Chemical Engineering, Nanchang University, Nanchang 330031, Jiangxi, China. [4]School for Engineering of Matter, Transport and Energy, Arizona State University, 551 E. Tyler Mall, Tempe, AZ 85287, USA.
*Corresponding author. Email: xinghb@zju.edu.cn

C_2H_4 and effectively impedes the diffusion of C_2H_6, inducing an outstanding recognition ability to C_2H_4 over C_2H_6. The equilibrium-kinetic combined selectivity (32.4), as well as C_2H_4 capacity of $ZnAtzPO_4$, outperforms those of the state-of-the-art materials. The extraordinary performance was achieved along with ultralow adsorption heat (17.3 kJ mol^{-1} for C_2H_4 at zero loading), and gas molecules adsorbed on the material can be easily removed at ambient temperature, indicating the promising prospect of the material for industrial application. DFT-D (dispersion-corrected density functional theory) calculations and molecular dynamics (MD) simulations were used to give insights into the unique separation mechanism, and breakthrough experiments for the C_2H_4/C_2H_6 (50:50, v/v) mixture were carried out to confirm the excellent performance of $ZnAtzPO_4$.

RESULTS

Pore structure and C_2H_4/C_2H_6 adsorption property

$ZnAtzPO_4$ was prepared by hydrothermal reaction of phosphoric acid, zinc carbonate basic, and Atz in a mixture of water, methanol, and aqueous ammonia under 180°C for 2 days (*34*). The structure of $ZnAtzPO_4$ contains two-dimensional cationic layers (fig. S1), which are fabricated by Zn^{2+} cations and deprotonated Atz ligands in both tridentate and bidentate coordination modes. The organic ligands only connect to Zn^{2+} cations via nitrogen atoms contained in the triazole rings, and the amino groups are all free of coordination. The layers are further pillared by PO_4^{3-} anions, resulting in the final porous framework of $ZnAtzPO_4$. As shown in Fig. 1A and fig. S1, the channel of $ZnAtzPO_4$ is decorated by intruding amino groups from bidentate-coordinated Atz ligands (highlighted by rose), which are arranged in an antiparallel manner along *a*, and abundant electronegative oxygen atoms from PO_4^{3-} anion pillars alongside the channel. The pillars adopt a staggered fashion, periodically contracting and expanding the cross section of the channel (Fig. 1B); therefore, the channel can be vividly described as iterant pocket-like space interconnected by narrow bottleneck structure. The pocket-like space each contains two symmetric passages (Fig. 1C) with the same size of 4.94 Å, which is enough to accommodate both C_2H_4 and C_2H_6 guests. In contrast, the neck is much narrower (3.82 Å, distance between N…N; Fig. 1D), which is quite close to the minimum dimension of C_2H_6 (3.81 Å) but apparently larger than that of C_2H_4 (3.28 Å). We anticipated that this delicate pocket-like structure would facilitate C_2H_4 trapping, but the narrow bottleneck would probably set a barrier for C_2H_6 to diffuse in the channel of $ZnAtzPO_4$.

Inspired by the eligible structure of $ZnAtzPO_4$, we further analyzed its thermodynamic and kinetic adsorption characteristics for C_2H_4 and C_2H_6 by measuring single-component adsorption isotherms and time-dependent gas uptake profiles. From the adsorption isotherms shown in Fig. 2A, $ZnAtzPO_4$ has a C_2H_4 uptake of 1.92 mmol g^{-1} at 298 K and 1 bar, equivalent to 3.04 mmol cm^{-3} (table S1). The adsorption capacity of C_2H_4 is higher than C_2H_6 in the whole pressure range, indicative of its preferable thermodynamic affinity for C_2H_4. The C_2H_4/C_2H_6 uptake ratio reached 1.85 at 1 bar, exceeding that of some excellently performing equilibrium-based porous materials for C_2H_4/C_2H_6 separation, such as HKUST-1 (1.19) (*35*), zeolite 5A (1.42) (*36*), and PAF-1-SO_3Ag (1.82) (*5*). As the temperature reduced to 273 K, the gas uptake ratio further increased to 2.04, and the amount of C_2H_4 captured attained 2.41 mmol g^{-1}. Meanwhile, kinetic studies suggested that the material exhibited much faster adsorption rate for C_2H_4 than C_2H_6. As shown in Fig. 2B, the adsorption of C_2H_4 reached equilibrium within about 40 min at 298 K and about 45 min at 273 K, with the capacities consistent to those taken from adsorption isotherms. After a continuous recording for 150 min, the amount of C_2H_6 adsorbed on the sample still has not reached that under the equilibrium state and persists climbing up gradually. Fitting the data with micropore diffusion model gave a kinetic selectivity of 36.6 at 298 K and up to 140.7 at 273 K (table S1), highlighting the potential of $ZnAtzPO_4$ to separate the C_2H_4/C_2H_6 mixture through a unique equilibrium-kinetic synergetic effect, which has rarely been observed in MOFs (*37*). To objectively compare the separation performance of $ZnAtzPO_4$ with other adsorbents ever reported for C_2H_4/C_2H_6 separation, we further calculated the equilibrium-kinetic combined selectivity (*38*) based on their diffusivities and Henry's constants for C_2H_4 and C_2H_6 gases. As shown in Fig. 2C and table S1, $ZnAtzPO_4$ displays a dramatic combined selectivity reaching up to 32.4 at 273 K. At ambient temperature, the selectivity is calculated as 12.4, higher than those of other kinetically selective adsorbents measured under similar conditions, like ITQ-29 (~1.31), Si-CHA (~1.31), and ITQ-55 (~6.4) (*31*, *32*).

To evaluate the strength of interactions between $ZnAtzPO_4$ and C_2H_4/C_2H_6 gases, the isosteric heat of adsorption (Q_{st}) was calculated for C_2H_4 and C_2H_6 based on their adsorption isotherms under three different temperatures using the Clausius-Clapeyron equation (fig. S2).

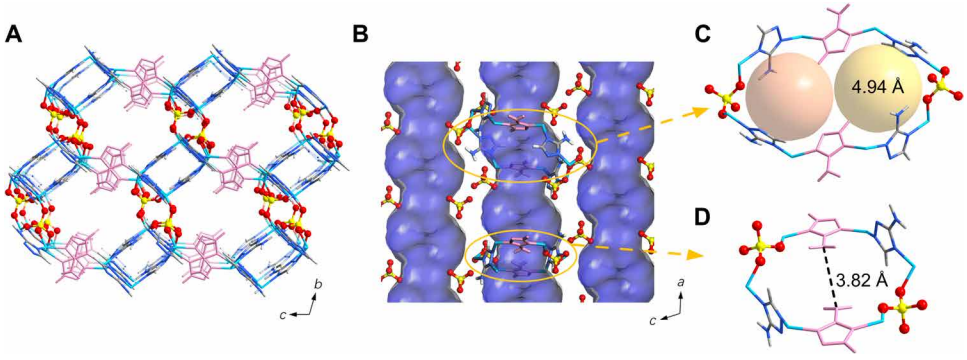

Fig. 1. Schematic illustration of the structure of $ZnAtzPO_4$. (**A**) Three-dimensional structure of $ZnAtzPO_4$ viewed from *a*. (**B**) Connolly surface indicating periodically expanded and contracted cross-section area of $ZnAtzPO_4$. (**C**) Schematic representation of the pocket-like space containing two symmetric passages. (**D**) Local environment and aperture size of the narrow bottleneck structure. [Color mode: C, gray (40%); H, gray (25%); N, light blue; Zn, sky blue; P, yellow; O, red. Bidentate-coordinated Atz ligands are highlighted by rose.]

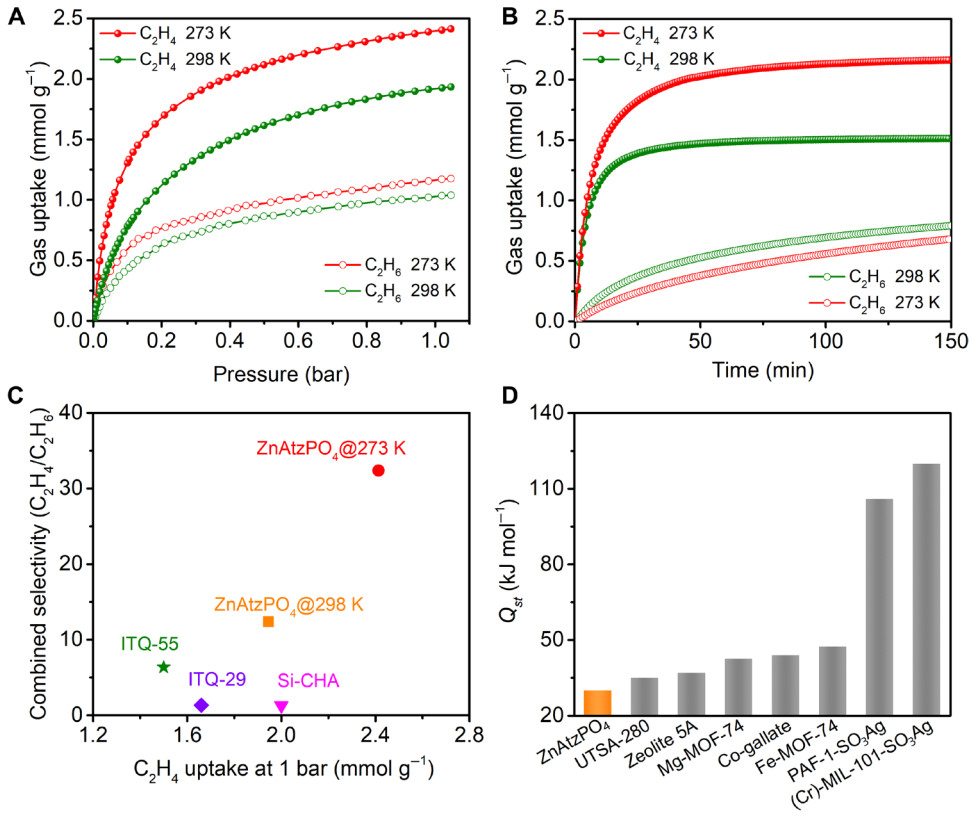

Fig. 2. Single-component gas adsorption properties. (**A**) Single-component adsorption isotherms of C_2H_4 and C_2H_6 on $ZnAtzPO_4$ under 298 and 273 K. (**B**) Time-dependent gas uptake profiles of C_2H_4 and C_2H_6 at 0.4 bar and different temperatures. (**C**) Equilibrium-kinetic combined selectivity (C_2H_4/C_2H_6) and C_2H_4 uptake of $ZnAtzPO_4$, ITQ-29, Si-CHA, and ITQ-55. Data for ITQ-55 were collected at 303 K, and those for ITQ-29 and Si-CHA were collected at 301 K. (**D**) Highest value of Q_{st} calculated for C_2H_4 on $ZnAtzPO_4$, UTSA-280, zeolite 5A, Mg-MOF-74, Co-gallate, Fe-MOF-74, PAF-1-SO_3Ag, and (Cr)-MIL-101-SO_3Ag.

The material exhibits moderate Q_{st} for C_2H_4, with the value varying from 17.31 to 29.98 kJ mol^{-1}. It is worth mentioning that the maximum value of Q_{st} for C_2H_4 is remarkably lower than those of UTSA-280 (35.0 kJ mol^{-1}) (*24*), zeolite 5A (37 kJ mol^{-1}) (*36*), Co-gallate (44 kJ mol^{-1}) (*3*), and many other adsorbents containing transition-metal ions and unsaturated metal sites, such as Mg-MOF-74 (42.6 kJ mol^{-1}) (*39*), Fe-MOF-74 (47.5 kJ mol^{-1}) (*20*), PAF-1-SO_3Ag (106 kJ mol^{-1}) (*5*), and (Cr)-MIL-101-SO_3Ag (120 kJ mol^{-1}) (*21*) (Fig. 2D). The moderate heat of adsorption reveals the possibility to regenerate this material under mild conditions; thereby, oligomerization of C_2H_4 that may happen under the catalysis of open metal sites could be avoided. For equilibrium-based adsorbents, the effective adsorption separation of C_2H_4 and C_2H_6 principally relies on the discrepancy between the affinities of the gases to the adsorbent; here, usually high isosteric heat is required for the preferentially adsorbed guest to achieve desirable selectivity. In the case of $ZnAtzPO_4$, the excellent selectivity achieved under the modest Q_{st} largely owns its way to exploit the synergetic effect of equilibrium and kinetics, which means that the separation capability of $ZnAtzPO_4$ is only partially reliant on thermodynamics. The kinetic characteristics of $ZnAtzPO_4$ also contribute to maximize the purification performance, without affecting the adsorption heat.

Besides, $ZnAtzPO_4$ presents great stability to air and moisture. After the sample was exposed to humid atmosphere (298 K, 70% humidity) for 4 weeks, no obvious change in its powder x-ray diffractometry (PXRD) pattern could be observed as compared to the as-synthesized sample (fig. S3). C_2H_4/C_2H_6 adsorption isotherms and time-dependent gas uptakes measured on the sample revealed that, after such treatment, their sorption properties still remained almost unchanged (fig. S3). Furthermore, thermal gravimetric analysis (TGA) indicates that this material exhibits excellent thermal stability, with the decomposition temperature approaching 420°C (fig. S4). These results qualify $ZnAtzPO_4$ as a promising candidate for industrial separation of C_2H_4 and C_2H_6.

Exploring separation mechanism by computational method

To gain insights into the unusual equilibrium-kinetic synergetic effect of $ZnAtzPO_4$ to effectively adsorb C_2H_4, first-principles DFT-D calculations were conducted to explore the preferential binding sites. The computational results demonstrate that $ZnAtzPO_4$ provides two distinct binding sites for C_2H_4 (Fig. 3, A and B). The capacious pocket-like space each contains two symmetric apertures (Fig. 1C), and they offer identical binding site (site I) to the olefin and can be reckoned as molecule traps. In this site, C_2H_4 molecule interacts with the channel mainly through weak hydrogen bonding interactions (Fig. 3A). It locates close to the pillaring PO_4^{3-} anions and bonds to the surrounding oxygen atoms from three different pillars via C—H…O hydrogen bonds. The shortest C—H…O bond has a length of 2.65 Å, while the others are longer and range from 2.90 to 3.16 Å. In addition, the C_2H_4 guest also strengthens its interaction with $ZnAtzPO_4$ by forming C—H…N hydrogen bonds with nitrogen atom coming from both amino group and triazole ring of the

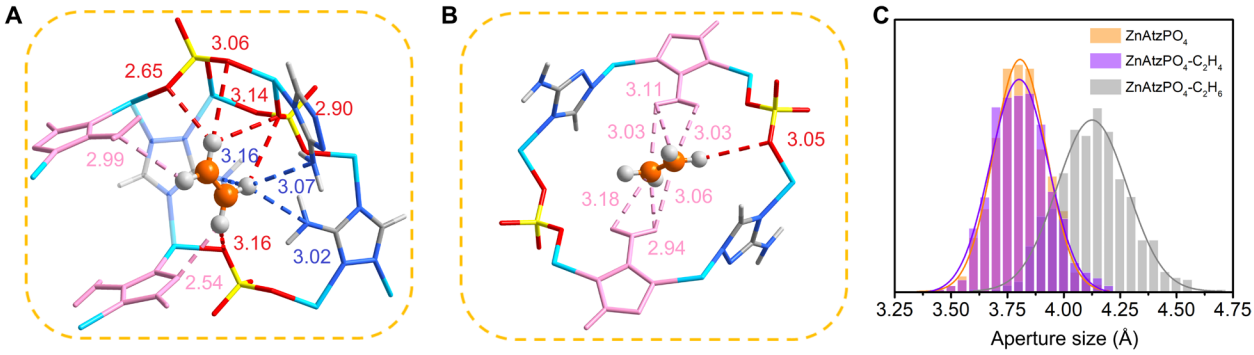

Fig. 3. DFT-D–calculated preferable binding sites for C_2H_4 in $ZnAtzPO_4$ and distribution of the aperture size of the bottleneck calculated from MD simulations. (**A**) Site I. (**B**) Site II. [Color mode: C, gray (40%); H, gray (25%); N, light blue; Zn, sky blue; P, yellow; O, red. Bidentate-coordinated Atz ligands are highlighted by rose. Broken lines refer to C—H…N/O hydrogen bonds and supermolecular N—H…C interactions. All interatomic distances are in angstroms.] (**C**) Distribution of the aperture size of the bottleneck for empty structure of $ZnAtzPO_4$ (orange), $ZnAtzPO_4$ with C_2H_4 molecules (violet), and $ZnAtzPO_4$ with C_2H_6 molecules (gray) at 298 K.

Atz ligands, with lengths of 2.54 to 3.16 Å. The second binding site (site II, Fig. 3B) for C_2H_4 is near the center of the bottleneck structure, which joins two adjacent pockets. The mechanism for C_2H_4 to interact with the adsorbent in this site is quite different from that in site I (Fig. 3A), where the molecular interactions are mainly dominated by hydrogen bonds. In site II, there is only one quite weak C—H…O bond formed between C_2H_4 and the PO_4^{3-} pillar, with the length being 3.05 Å. Because of the specific chemical environment, the adsorbate is mainly stabilized by supermolecular N—H…C interactions with hydrogen atoms of the intruding amino groups from the bidentate-coordinated Atz ligands, and their lengths are in the range of 2.94 to 3.18 Å. The fact that there is a lack of strong hydrogen bond (C—H…O/N < 2.3 Å) (*2*) in sites I and II proves that the adsorbate merely interacts with the pore through weak intermolecular interactions, consistent to the quite modest value of Q_{st} as has been calculated. Furthermore, the DFT-D study on C_2H_6 reveals that unlike C_2H_4, the C_2H_6 molecule can only approach the binding site in the capacious pocket-like space (fig. S5). The molecular dimension of C_2H_6 is comparable to the size of the bottleneck structure, and it induces a steric hindrance to prevent the bottleneck to expose the second binding site to C_2H_6. The distinct modes between C_2H_4 and C_2H_6 to interact with the pore may be the reason that endows $ZnAtzPO_4$ with the excellent thermodynamic selectivity.

The diffusion behaviors of C_2H_4 and C_2H_6 in the pore of $ZnAtzPO_4$ were further investigated by performing MD simulations to reveal the kinetic characteristics. The simulations demonstrate that, when each cell of $ZnAtzPO_4$ contains two gas molecules, the diffusivities of single-component C_2H_4 and C_2H_6 are 2.07×10^{-10} m^2 s^{-1} and 7.17×10^{-12} m^2 s^{-1} under 298 K. The ideal kinetic selectivity is calculated as 29 and agrees well with the experimental measurement (~36). For the equimolar C_2H_4/C_2H_6 gas mixture, the diffusivities of C_2H_4 and C_2H_6 are 1.12×10^{-10} m^2 s^{-1} and 7.47×10^{-12} m^2 s^{-1}, respectively. Although the adsorption kinetics of C_2H_4 in the mixture declines as compared to its single component maybe due to the steric effect of slow-diffusing C_2H_6, the material still exhibits a prominent kinetic selectivity of 15. The results also indicate that after introducing C_2H_6 molecules to the channel of $ZnAtzPO_4$, the bottleneck exhibits obvious transient structural transformations to adapt to the sluggish passing of C_2H_6, and the aperture size prominently increases to 4.1 Å, about 0.3 Å larger than that without gas molecules (Fig. 3C). Snapshots (fig. S6) show that the expansion of the bottleneck-like window is mainly facilitated by slight rotation of the bidentate-coordinated Atz ligands that intrude amino groups to the channel. On the contrary, study on the diffusion of C_2H_4 reveals that after inserting the gas molecule to the channel, no obvious change in the aperture size of the bottleneck was observed, and its probability distribution is quite consistent to that of an empty host (Fig. 3C). These results suggest that the diffusion of C_2H_6 in the channel strongly relies on the flexibility of $ZnAtzPO_4$, considering that the size of the bottleneck (3.82 Å) at the ground state is so close to the extreme size (3.81 Å) to allow the passing of C_2H_6, setting a barrier for its penetration. The much smaller dimension of C_2H_4 (3.28 Å) allows it to travel along the pore more freely, without the necessity to expand the narrow windows, which thereby induces the marked kinetic selectivity of $ZnAtzPO_4$.

Breakthrough experiments

It is worth emphasizing that removal of C_2H_6 from C_2H_4 is yet a technical challenge in industry. To further probe the validity of the equilibrium-kinetic synergetic effect for C_2H_4/C_2H_6 separation, breakthrough experiments for a C_2H_4/C_2H_6 (50:50, v/v) gas mixture were performed on a stainless column packed with the $ZnAtzPO_4$ material at 273 K and 1 bar. As shown in Fig. 4A, the component of C_2H_6 broke through the column quickly after 26 min, whereas C_2H_4 was retained in the adsorption bed for nearly 70 min. The retention time for C_2H_4 is two times more than that of C_2H_6. Moreover, the elution of C_2H_4 was accompanied by a remarkable roll-up phenomenon of C_2H_6, meaning that the C_2H_6 molecules that have already been adsorbed can be largely displaced by the olefin, indicative of the excellent competition ability of C_2H_4 over C_2H_6 on the binding sites of $ZnAtzPO_4$. After the concentration of eluting gas remained unchanged, the amount of C_2H_4 adsorbed into the column reached 1.80 mmol g^{-1}, equivalent to 6.7 times that of C_2H_6 (0.27 mmol g^{-1}) (fig. S7), highlighting the great efficiency of $ZnAtzPO_4$ for actual C_2H_4/C_2H_6 adsorption separation. Besides, recycling measurements reveal that $ZnAtzPO_4$ can retain its separation capability, with the breakthrough time being almost unchanged within five cycles (Fig. 4B and fig. S7). After simple desorption procedure manipulated by purging the material with inert gas (He) at ambient temperature, the column was well regenerated and reserved similar breakthrough curve (fig. S7), benefitting from the very modest adsorption heat as has been calculated. This further presents $ZnAtzPO_4$ as a brilliant

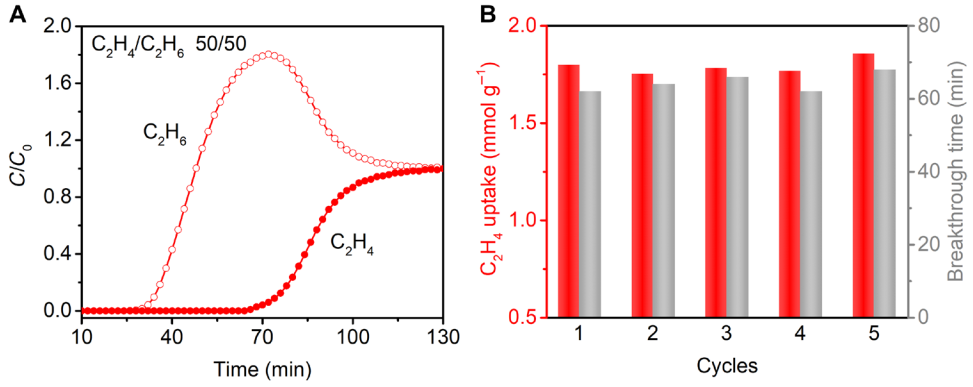

Fig. 4. Breakthrough curve and recycling tests for C_2H_4/C_2H_6 gas mixture on $ZnAtzPO_4$. (**A**) Breakthrough curve of $ZnAtzPO_4$ for C_2H_4/C_2H_6 gas mixture (50:50, v/v) at 273 K and 1 bar with a flow rate of 0.75 ml/min. (**B**) Recycling breakthrough tests for C_2H_4/C_2H_6 (50:50, v/v) separation with $ZnAtzPO_4$.

microporous material for industrial separation of C_2H_4 and C_2H_6. By exploiting the equilibrium-kinetic synergetic effect, we successfully achieved the high-efficient C_2H_4/C_2H_6 adsorption separation with $ZnAtzPO_4$. With the solid empirical evidence, we believe that it would bring a new train of thoughts and tactics for the splitting of close-boiling light hydrocarbons.

DISCUSSION

In summary, we reported the separation of C_2H_4/C_2H_6 in a phosphate-anion pillared microporous MOF, which exhibits a unique equilibrium-kinetic combined selectivity to the olefin and is attractive for practical separation. The equilibrium-kinetic synergetic effect of $ZnAtzPO_4$ mainly originates from its delicate pore structure, featuring periodically expanded and contracted cross section. Its minimum aperture size approaches the limit for C_2H_6 to pass through, and the diffusion of C_2H_6 depends on transient structural transformations of the neck-like structure, which seriously slows down the diffusion rate of the paraffin. On the other hand, the pore of $ZnAtzPO_4$ is decorated with abundant electronegative functional groups that are amenable to construct stable interaction network with C_2H_4 and trap the olefin efficiently. Computational methods were applied to explore the binding sites of the guest molecules and further verify the faster adsorption kinetics of C_2H_4. Moreover, recycling breakthrough experiment for the C_2H_4/C_2H_6 gas mixture (50:50, v/v) was carried out, and it confirmed the outstanding capability of $ZnAtzPO_4$ for C_2H_4/C_2H_6 separation.

As most porous materials ever reported for C_2H_4/C_2H_6 separation are typically based on single mechanism (either thermodynamic or kinetic), examples to explore synergetic effect of equilibrium and kinetics in this regard are rare. The unprecedented selectivity achieved on $ZnAtzPO_4$ proves that the strategy conveyed by this work is feasible and practical and highlights a broad space to further boost the adsorption separation of C_2H_4 and C_2H_6 in a newfangled way. Taking advantage of such synergetic effect allows highly efficient selective adsorption of C_2H_4 under modest Q_{st}, because the separation process only partially relies on thermodynamics. As a glaring merit, the material can be regenerated under mild conditions with less energy consumption. In brief, this work not only provides a porous material with impressive C_2H_4 purification performance but also brings a new strategy for developing the next-generation materials for energy-efficient gas separation.

MATERIALS AND METHODS

Experimental design

Chemicals

All the chemicals were obtained from commercial resources and used as received without any further purification. Methanol (anhydrous, 99%) was purchased from Sigma-Aldrich. Phosphoric acid [85 weight % (wt %)], ammonium hydroxide (30 wt %), and 3-amino-1,2,4-triazole (96%) were purchased from Macklin. $3Zn(OH)_2{\cdot}2ZnCO_3$ was purchased from Strem Chemicals.

Synthesis of $\{Zn_3(Atz)_3(PO_4)\}_\infty$ ($ZnAtzPO_4$)

Samples of $ZnAtzPO_4$ were synthesized according to the literature report (*34*) with minor modifications. A mixture containing 0.035 g of phosphoric acid, 0.1 g of $3Zn(OH)_2{\cdot}2ZnCO_3$, 0.4 g of 3-amino-1,2,4-triazole, 2 ml of H_2O, and 2 ml of methanol was added to a Teflon tube, then sealed and placed in an oven with a temperature of 180°C for 48 hours, and cooled to room temperature naturally. The colorless precipitation was collected by filtration, then washed with methanol, and dried in air. Last, the product was heated at 60°C under high vacuum for 2 hours and then at 100°C for another 12 hours to obtain the activated sample of $ZnAtzPO_4$.

Characterization methods

PXRD data were collected on a SHIMADZU XRD-600 diffractometer (Cu $K_\alpha\lambda$ = 1.540598 Å) with an operating power of 40 kV, 30 mA, and a scan speed of 4.0°/min. The range of 2θ was from 5° to 50°. TGA data for activated sample of $ZnAtzPO_4$ were recorded on an apparatus of TGA Q500 V20.13 Build 39, from room temperature to 800°C, with a ramp of 10°/min under N_2 atmosphere.

Kinetic adsorption measurement

The time-dependent adsorption profiles of C_2H_4 and C_2H_6 were measured on Intelligent Gravimetric Analyzer (IGA-100, HIDEN). About 100 mg of $ZnAtzPO_4$ was first loaded to the sample chamber and activated at 100°C under high vacuum for 4 hours. After being cooled to specific temperature, the chamber was backfilled with He, until the pressure reached 0.4 bar. Upon the analysis started, a single-component gas of C_2H_4 or C_2H_6 was introduced into the chamber at a rate of 35 ml/min. The mass of the sample loaded with gas molecules was continuously recorded for 150 min.

Statistical analysis

The equilibrium-kinetic combined selectivity (S_{ij}) is defined as (*38*)

$$S_{ij} = \alpha_{ij} \times \beta_{ij}^{0.5} \quad (1)$$

In Eq. 1, α_{ij} represents the separation selectivity based on thermodynamic equilibrium alone and can be calculated from the ratio of Henry's constants (Eq. 2). β_{ij} represents the kinetic selectivity based on diffusion rates of the gas molecules and can be obtained from the ratio of diffusion time constants (Eq. 3)

$$\alpha_{ij} = H_i/H_j \quad (2)$$

$$\beta_{ij} = D'_i/D'_j \quad (3)$$

In Eq. 3, D' (D_c/r_c^2) can be further derived from the following micropore diffusion model (Eq. 4), where m_t is the gas uptake at time t, m_∞ is the gas uptake at equilibrium, D_c is the intracrystalline diffusivity of gas molecules in porous media, and r_c is the radius of the equivalent spherical particle. D' can be obtained from the square of the slope ($\frac{m_t}{m_\infty}$ plotted against $\sqrt{t}$) multiplied by $\pi/36$

$$\frac{m_t}{m_\infty} \approx \frac{6}{r_c}\sqrt{\frac{D_C t}{\pi}} (m_t/m_\infty < 0.3) \quad (4)$$

SUPPLEMENTARY MATERIALS

Supplementary material for this article is available at http://advances.sciencemag.org/cgi/content/full/6/15/eaaz4322/DC1

REFERENCES AND NOTES

1. L. Li, R.-B. Lin, R. Krishna, H. Li, S. Xiang, H. Wu, J. Li, W. Zhou, B. Chen, Ethane/ethylene separation in a metal-organic framework with iron-peroxo sites. *Science* **362**, 443–446 (2018).
2. P.-Q. Liao, W.-X. Zhang, J.-P. Zhang, X.-M. Chen, Efficient purification of ethene by an ethane-trapping metal-organic framework. *Nat. Commun.* **6**, 8697 (2015).
3. Z. Bao, J. Wang, Z. Zhang, H. Xing, Q. Yang, Y. Yang, H. Wu, R. Krishna, W. Zhou, B. Chen, Q. Ren, Molecular sieving of ethane from ethylene through the minimum molecular dimension differentiation in gallate-based metal-organic frameworks. *Angew. Chem. Int. Ed. Engl.* **57**, 16020–16025 (2018).
4. M. Rungta, C. Zhang, W. J. Koros, L. Xu, Membrane-based ethylene/ethane separation: The upper bound and beyond. *AIChE J.* **59**, 3475–3489 (2013).
5. B. Li, Y. Zhang, R. Krishna, K. Yao, Y. Han, Z. Wu, D. Ma, Z. Shi, T. Pham, B. Space, J. Liu, P. K. Thallapally, J. Liu, M. Chrzanowski, S. Ma, Introduction of π-complexation into porous aromatic framework for highly selective adsorption of ethylene over ethane. *J. Am. Chem. Soc.* **136**, 8654–8660 (2014).
6. D. S. Sholl, R. P. Lively, Seven chemical separations to change the world. *Nature* **532**, 435–437 (2016).
7. J. Peng, H. Wang, D. H. Olson, Z. Li, J. Li, Efficient kinetic separation of propene and propane using two microporous metal organic frameworks. *Chem. Commun.* **53**, 9332–9335 (2017).
8. A. Cadiau, K. Adil, P. M. Bhatt, Y. Belmabkhout, M. Eddaoudi, A metal-organic framework-based splitter for separating propylene from propane. *Science* **353**, 137–140 (2016).
9. J.-R. Li, J. Sculley, H.-C. Zhou, Metal-organic frameworks for separations. *Chem. Rev.* **112**, 869–932 (2012).
10. B. Chen, C. Liang, J. Yang, D. S. Contreras, Y. L. Clancy, E. B. Lobkovsky, O. M. Yaghi, S. Dai, A microporous metal-organic framework for gas-chromatographic separation of alkanes. *Angew. Chem. Int. Ed. Engl.* **45**, 1390–1393 (2006).
11. X. Cui, K. Chen, H. Xing, Q. Yang, R. Krishna, Z. Bao, H. Wu, W. Zhou, X. Dong, Y. Han, B. Li, Q. Ren, M. J. Zaworotko, B. Chen, Pore chemistry and size control in hybrid porous materials for acetylene capture from ethylene. *Science* **353**, 141–144 (2016).
12. L. Yang, X. Cui, Q. Yang, S. Qian, H. Wu, Z. Bao, Z. Zhang, Q. Ren, W. Zhou, B. Chen, H. Xing, A single-molecule propyne trap: Highly efficient removal of propyne from propylene with anion-pillared ultramicroporous materials. *Adv. Mater.* **30**, 1705374 (2018).
13. Z. Zhang, Q. Yang, X. Cui, L. Yang, Z. Bao, Q. Ren, H. Xing, Sorting of C4 olefins with interpenetrated hybrid ultramicroporous materials by combining molecular recognition and size-sieving. *Angew. Chem. Int. Ed.* **129**, 16500–16505 (2017).
14. Q.-G. Zhai, X. Bu, C. Mao, X. Zhao, L. Daemen, Y. Cheng, A. J. Ramirez-Cuesta, P. Feng, An ultra-tunable platform for molecular engineering of high-performance crystalline porous materials. *Nat. Commun.* **7**, 13645 (2016).
15. Z.-J. Zhang, W. Shi, Z. Niu, H.-H. Li, B. Zhao, P. Cheng, D.-Z. Liao, S. P. Yan, A new type of polyhedron-based metal-organic frameworks with interpenetrating cationic and anionic nets demonstrating ion exchange, adsorption and luminescent properties. *Chem. Commun.* **47**, 6425–6427 (2011).
16. X.-H. Bu, M.-L. Tong, H.-C. Chang, S. Kitagawa, S. R. Batten, A neutral 3D copper coordination polymer showing 1D open channels and the first interpenetrating NbO-type network. *Angew. Chem. Int. Ed.* **43**, 192–195 (2004).
17. S. Aguado, G. Bergeret, C. Daniel, D. Farrusseng, Absolute molecular sieve separation of ethylene/ethane mixtures with silver zeolite A. *J. Am. Chem. Soc.* **134**, 14635–14637 (2012).
18. U. Böhme, B. Barth, C. Paula, A. Kuhnt, W. Schwieger, A. Mundstock, J. Caro, M. Hartmann, Ethene/ethane and propene/propane separation via the olefin and paraffin selective metal-organic framework adsorbents CPO-27 and ZIF-8. *Langmuir* **29**, 8592–8600 (2013).
19. S. Uchida, R. Kawamoto, H. Tagami, Y. Nakagawa, N. Mizuno, Highly selective sorption of small unsaturated hydrocarbons by nonporous flexible framework with silver ion. *J. Am. Chem. Soc.* **130**, 12370–12376 (2008).
20. E. D. Bloch, W. L. Queen, R. Krishna, J. M. Zadrozny, C. M. Brown, J. R. Long, Hydrocarbon separations in a metal-organic framework with open iron(II) coordination sites. *Science* **335**, 1606–1610 (2012).
21. G. Chang, M. Huang, Y. Su, H. Xing, B. Su, Z. Zhang, Q. Yang, Y. Yang, Q. Ren, Z. Bao, B. Chen, Immobilization of Ag(I) into a metal-organic framework with -SO_3H sites for highly selective olefin-paraffin separation at room temperature. *Chem. Commun.* **51**, 2859–2862 (2015).
22. A. Cadiau, Y. Belmabkhout, K. Adil, P. M. Bhatt, R. S. Pillai, A. Shkurenko, C. Martineau-Corcos, G. Maurin, M. Eddaoudi, Hydrolytically stable fluorinated metal-organic frameworks for energy-efficient dehydration. *Science* **356**, 731–735 (2017).
23. L. Li, R.-B. Lin, X. Wang, W. Zhou, L. Jia, J. Li, B. Chen, Kinetic separation of propylene over propane in a microporous metal-organic framework. *Chem. Eng. J.* **354**, 977–982 (2018).
24. R.-B. Lin, L. Li, H.-L. Zhou, H. Wu, C. He, S. Li, R. Krishna, J. Li, W. Zhou, B. Chen, Molecular sieving of ethylene from ethane using a rigid metal–organic framework. *Nat. Mater.* **17**, 1128–1133 (2018).
25. P. Nugent, Y. Belmabkhout, S. D. Burd, A. J. Cairns, R. Luebke, K. Forrest, T. Pham, S. Ma, B. Space, L. Wojtas, M. Eddaoudi, M. J. Zaworotko, Porous materials with optimal adsorption thermodynamics and kinetics for CO_2 separation. *Nature* **495**, 80–84 (2013).
26. Y. Wang, N.-Y. Huang, X.-W. Zhang, H. He, R.-K. Huang, Z.-M. Ye, Y. Li, D.-D. Zhou, P.-Q. Liao, X.-M. Chen, J.-P. Zhang, Selective aerobic oxidation of a metal-organic framework boosts thermodynamic and kinetic propylene/propane selectivity. *Angew. Chem. Int. Ed. Engl.* **58**, 7692–7696 (2019).
27. R.-B. Lin, H. Wu, L. Li, X.-L. Tang, Z. Li, J. Gao, H. Cui, W. Zhou, B. Chen, Boosting ethane/ethylene separation within isoreticular ultramicroporous metal-organic frameworks. *J. Am. Chem. Soc.* **140**, 12940–12946 (2018).
28. Y. Wang, S. Yuan, Z. Hu, T. Kundu, J. Zhang, S. B. Peh, Y. Cheng, J. Dong, D. Yuan, H.-C. Zhou, D. Zhao, Pore size reduction in zirconium metal–organic fameworks for ethylene/ethane separation. *ACS Sustainable Chem. Eng.* **7**, 7118–7126 (2019).
29. Z. Bao, G. Chang, H. Xing, R. Krishna, Q. Ren, B. Chen, Potential of microporous metal–organic frameworks for separation of hydrocarbon mixtures. *Energ. Environ. Sci.* **9**, 3612–3641 (2016).
30. S. Yang, A. J. Ramirez-Cuesta, R. Newby, V. Garcia-Sakai, P. Manuel, S. K. Callear, S. I. Campbell, C. C. Tang, M. Schröder, Supramolecular binding and separation of hydrocarbons within a functionalized porous metal–organic framework. *Nat. Chem.* **7**, 121–129 (2015).
31. P. J. Bereciartua, Á. Cantín, A. Corma, J. L. Jordá, M. Palomino, F. Rey, S. Valencia, E. W. Corcoran Jr, P. Kortunov, P. I. Ravikovitch, A. Burton, C. Yoon, Y. Wang, C. Paur, J. Guzman, A. R. Bishop, G. L. Casty, Control of zeolite framework flexibility and pore topology for separation of ethane and ethylene. *Science* **358**, 1068–1071 (2017).
32. N. Hedin, G. J. Demartin, W. J. Roth, K. G. Strohmaier, S. C. Reyes, PFG NMR self-diffusion of small hydrocarbons in high silica DDR, CHA and LTA structures. *Microporous Mesoporous Mater.* **109**, 327–334 (2008).
33. C. Gu, N. Hosono, J.-J. Zheng, Y. Sato, S. Kusaka, S. Sakaki, S. Kitagawa, Design and control of gas diffusion process in a nanoporous soft crystal. *Science* **363**, 387–391 (2019).
34. R. Vaidhyanathan, S. S. Iremonger, G. K. H. Shimizu, P. G. Boyd, S. Alavi, T. K. Woo, Competition and cooperativity in carbon dioxide sorption by amine-functionalized metal-organic frameworks. *Angew. Chem. Int. Ed.* **51**, 1826–1829 (2012).
35. Y. He, R. Krishna, B. Chen, Metal-organic frameworks with potential for energy-efficient adsorptive separation of light hydrocarbons. *Energ. Environ. Sci.* **5**, 9107–9120 (2012).
36. M. Mofarahi, S. M. Salehi, Pure and binary adsorption isotherms of ethylene and ethane on zeolite 5A. *Adsorption* **19**, 101–110 (2013).
37. Z. Bao, S. Alnemrat, L. Yu, I. Vasiliev, Q. Ren, X. Lu, S. Deng, Kinetic separation of carbon dioxide and methane on a copper metal-organic framework. *J. Colloid Interface Sci.* **357**, 504–509 (2011).
38. R. T. Yang, *Adsorbents: Fundamentals and Applications* (Wiley-Interscience, 2003).
39. Z. Bao, S. Alnemrat, L. Yu, I. Vasiliev, Q. Ren, X. Lu, S. Deng, Adsorption of ethane, ethylene, propane, and propylene on a magnesium-based metal-organic framework. *Langmuir* **27**, 13554–13562 (2011).

Acknowledgments
Funding: This work was supported by the National Natural Science Foundation of China (nos. 21938011, 21725603, and U1862110), the Zhejiang Provincial Natural Science Foundation of China (no. LZ18B060001), and the National Supercomputing Center in Shenzhen. **Author contributions:** Q.D. carried out the experimental work on synthesis, adsorption isotherm measurements, and breakthrough tests and performed the computational simulations. Z.Z. and C.Y. took part in synthesis and recycling tests. P.Z., J.W., and S.D. measured time-dependent gas uptake profiles of C_2H_4 and C_2H_6. X.C. and C.-H.H. took part in modeling studies. H.X. and Q.D. conceived the idea and analyzed the results. All authors contributed to the final version of the manuscript. **Competing interests:** H.X., X.C., and Q.D. are inventors on a patent related to this work filed by Zhejiang University (no. 201910084873.8, filed on 29 January 2019). The authors declare no other competing interests. **Data and materials availability:** All data needed to evaluate the conclusions in the paper are present in the paper and/or the Supplementary Materials.

Submitted 9 September 2019
Accepted 15 January 2020
Published 10 April 2020
10.1126/sciadv.aaz4322

Citation: Q. Ding, Z. Zhang, C. Yu, P. Zhang, J. Wang, X. Cui, C.-H. He, S. Deng, H. Xing, Exploiting equilibrium-kinetic synergetic effect for separation of ethylene and ethane in a microporous metal-organic framework. *Sci. Adv.* **6**, eaaz4322 (2020).